Proceedings of the ASME 2015 34th International Conference on Ocean, Offshore and Arctic Engineering
OMAE2015
May 31-June 5, 2015, St. John's, Newfoundland, Canada

OMAE2015-41892

DRAFT: THE PHYSICAL BEHAVIOUR OF SEINE ROPES FOR EVALUATING DEMERSAL SEINE FISHING

Nina A. H. Madsen[1]
SINTEF
Fisheries and Aquaculture
Hirtshals, Denmark
nina.madsen@sintef.no

Karl Gunnar Aarsæther
SINTEF
Fisheries and Aquaculture
Trondheim, Norway

Bent Herrmann
SINTEF
Fisheries and Aquaculture
Hirtshals, Denmark

Kurt Hansen
SINTEF
Fisheries and Aquaculture
Hirtshals, Denmark

Jørgen H. Jensen
SINTEF
Fisheries and Aquaculture
Trondheim, Norway

ABSTRACT

Demersal seining is an active bottom fishing method, which apply seine ropes and a seine net. The seine ropes and net are laid out on the fishing ground with the seine ropes encircling an aggregation of fish on the seabed. The area on the seabed encircled by the seine ropes is typical much larger than the swept area that will be covered by the seine net during the fishing process. Therefore, the catching performance of a demersal seine depends on the efficiency by which the seine ropes are able to herd the fish into and maintain them in the path of the net until they are overtaken by it in the late stages of the fishing process. This article describes flume tank experiments to validate a numerical model. This model simulates the physical behaviour of seine ropes during the fishing process. The experiments are conducted for varying physical properties of the ropes and for different layout patterns. The seine ropes are hauled back at different speeds. A motion tracking system, based on stereo vision, is applied to record the gradual change in the area encircled by the ropes. The experimental results from the flume tank are compared with data obtained using the simulation model. Finally, the validated simulation model is applied for predictions.

NOMENCLATURE

$\dot{\boldsymbol{x}}, \ddot{\boldsymbol{x}}$	First and second derivative with respect to time of $\boldsymbol{x}$
$\boldsymbol{b}$	Element vector
$\boldsymbol{C}$	Constraint
$\boldsymbol{f}$	Force in inertial frame
$\boldsymbol{h}$	Angular momentum
K_{dL}	Constraint stabilizing feedback derivative gain
K_{pL}	Constraint stabilizing feedback proportional gain
L	Element length
m	Element mass
$\boldsymbol{n}$	Element end point position
$\boldsymbol{q}$	Constraint degree of freedom
$\boldsymbol{r}$	Element centre position
$\boldsymbol{u}_l$	Feedback force for to correct constraint equation drift
V	Volume of element
$\boldsymbol{W}$	Constraint derivative with respect to degree of freedom
ζ	Element coordinate in angular momentum calculation
ρ	Density of material or fluid

INTRODUCTION

Worldwide demersal seining is a commonly applied fishing method to harvest species that live close to the seabed. E.g. in Norwegian fishery; cod is the most important species in the white fish fishery when measured in both tonnes landed and in value [1]. About 20% of the Norwegian cod quota is caught by demersal seining; the Norwegian style fly dragging. Thus, knowledge about the physical behaviour of this type of gear is very relevant. Demersal seining in Norwegian fishery targeting cod and other demersal species is practiced by deploying two long seine ropes connected to the wing tips of the seine net in one end and the winches of the vessel on the other end. The

[1] Address all correspondence to this author.

length of the seine ropes is restricted to 2000 m each when fishing inside the four nautical mile limit. The seine ropes, made of up to Ø60 mm combination rope (polyethylene with a steel core) weighting more than 2 kg/m, are placed on the seabed in a quadrilateral pattern in order to encircle the targeted fish [2]. Once the ropes and the net have reached the seabed the vessel starts moving forward at a speed of 1-1.5 knots. As a result of the vessel movement the seine ropes are moving towards each other and herd the fish into the centre of the encircled area; the collecting phase. At some instance the net will start to move along the seabed when pulled by the seine ropes. When the distance between the ropes has decreased to a certain level the rope drums are activated in order to close the wings fast and to force the last fraction of collected fish into the seine net; the closing phase. This fly dragging principle of demersal seining is shown in Fig. 1.

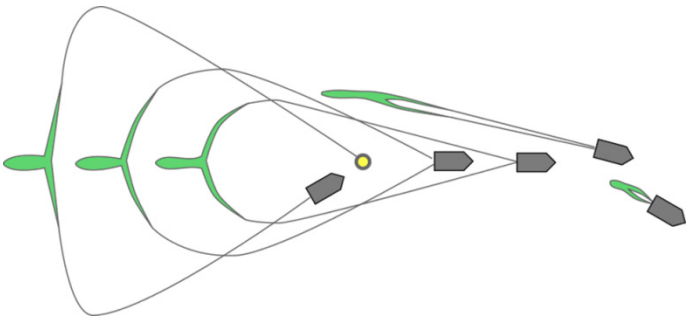

FIGURE 1: Demersal seine fishing procedure [3]

Underwater observations [4] have confirmed that fish starts entering the funnel of the net as soon as the seine net is sat in motion during the collecting phase. However, the majority of those fish herded by the ropes enter the belly and codend of the seine net in the later stages of the closing phase. The actual fishing time, i.e. the collecting and closing phases, may be as short as 15 minutes. The area on the seabed encircled by the seine ropes is typical much larger than the swept area that will be covered by the seine net during the fishing process. Therefore the catching performance of a demersal seine fishing operation depends to a large extent on the efficiency by which the seine ropes are able to herd the fish into and subsequently maintain them in the path of the net until they are overtaken by it in the later stages of the fishing process. Knowledge about how the size and shape of the area encircled by the seine ropes gradually change during the fishing process is therefore important for an efficient fishery. Thus, being able to model the physical behaviour of the seine ropes is an important aspect of simulating the demersal seine fishing process. It is necessary with experimental data for validation in order to be able to develop a reliable simulation model for the physical behaviour of seine ropes. This article describe flume tank experiments carried out to obtain data for seine rope behaviour. A seine ropes simulation model is then outlined and simulated results are compared to similar experimentally obtained in the flume tank. Finally, the validated simulation model is applied for predictions.

MATERIALS AND METHODS

Flume Tank Measuring Principle

The experiments were conducted in the SINTEF operated flume tank [5, 6] in Hirtshals, Denmark. The measuring section of the tank is 21.3 m long and 8 m wide, with a water depth of 2.7 m. The volume of water is 1200 m^3. To measure the shape of the seine ropes in the flume tank continuously during the haul back procedure we applied the motion tracking system installed in the flume tank. This system is based on hardware and software from the Swedish company Qualisys AB [7]. The measuring principle in the system is based on stereo vision techniques using six underwater cameras of the type ”Oqus Underwater”. Four of the cameras are mounted on a beam in the aft of the flume tank while the two others are on a second beam further forward in the tank. The object under investigation is being equipped with a number of reflective markers. In the current case, the seine ropes. Each camera emits a blue stroboscope light by LEDs build into each of the cameras in a circular arrangement. The emitted blue light is then reflected on the surface of the markers back to the camera to provide 2D positions in camera coordinate. The maximum sampling frequency of the system is more than 100 Hz and the system can follow more than 200 reflective markers [7]. Extracting 3D coordinates for a marker requires that at least two of the six cameras simultaneously acquire the 2D position for the marker. Thus 3D motion tracking of the target object occurs only at the points where markers are located on the object. The markers we used for the experiment consist of a spherical body (diameter of 32 mm) covered in a retro-reflective tape designed to work underwater. Fig. 2 illustrates the measuring principle applied.

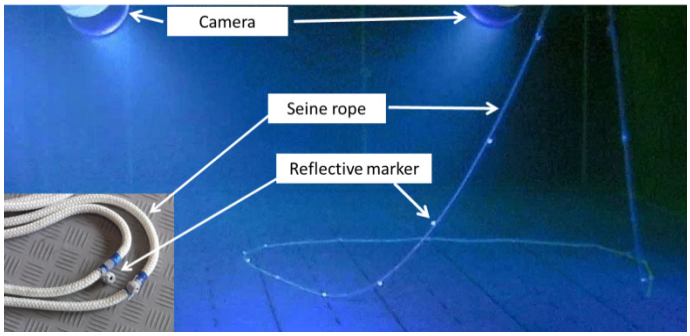

FIGURE 2: Photo from the flume tank illustrating the data acquisition principle. The insert shows the reflective markers sewn onto the rope.

For the motion tracking we mounted 23 reflective markers on the seine ropes along the length. The distance along the ropes between neighbouring markers was approximately 1.0 m except for between two pairs of the markers where the distance was 0.5 m to obtain a better resolution on the motion of the

seine ropes near the corners of the initial layout patterns. The data acquisition method illustrated in Fig. 2 was used for simultaneous capture of 2D camera positions for all of the reflective markers in the field of view obtained with the six underwater cameras. These were then processed in the Qualisys analysis software using the stereo vision principle [8] to obtain the simultaneous 3D geometrical coordinates for the position of all the reflective markers mounted on the ropes. The 3D positions of the reflective markers on the seine ropes were acquired with a frequency of 10 Hz during the haul back procedure. The Qualisys analysis software was used to produce a time trace of the position for each of the markers during the process. Fig. 3 illustrates this time trace with a screen dump from the Qualisys analysis software.

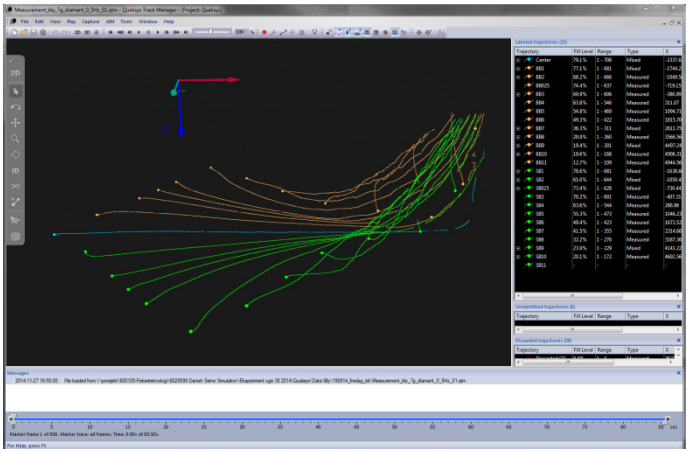

FIGURE 3: Screen dump of the Qualisys software, showing the time traces of the movement for the individual markers during the haul back of the seine ropes

Based on the time traces of the reflective markers placed on the seine ropes (Fig. 3) we processed the data further to produce a sequence of 2D pictures of how the shape of the seine ropes gradually change during the haul back process. We produced this sequence of the kinematic behaviour of the ropes seen from above and from the side. This type of information is later to be overlaid with similar plots obtained from simulations, with the purpose to be able to validate the simulation model.

An electricity driven winch was mounted on the bridge of the flume tank and applied to conduct the haul back of the seine ropes. A frequency convertor controls the winch speeds. During the experiments we conducted the same haul back cases with two different winch speeds at respectively 0.5 Hz (15.7 cm/s) and 1.0 Hz (31.4 cm/s).

The seine ropes were laid out on the flume tank floor in a specific pattern before starting the haul back process. Since the seine ropes behaviour might be different for different initial layout patterns we acquired motion tracking data for three different: square, diamond and triangle (Fig. 4).

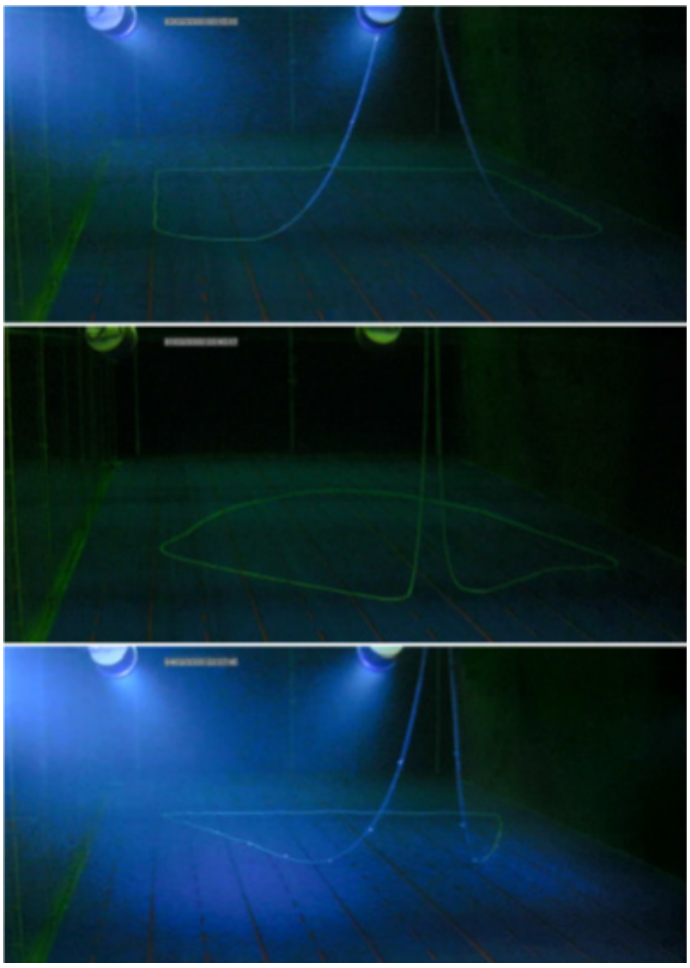

FIGURE 4: Photos of the three initial layout patterns applied in the flume tank experiments. From top: square, diamond and triangle.

Experimental Cases for the Flume Tank Test

Two types of ropes with considerable different densities were applied in order to investigate its effect on the shape encircled by the seine ropes during the haul back process:

- Light weight polyester rope with diameter 14 mm and a weight of 0.18 Kg per meter rope.
- Heavy combinations rope with a lead core and a polyester cover. The diameter was 14 mm and a weight of 0.5 Kg per meter rope.

The ropes were 30 m long (15 m per seine rope) and both types had a very small bending stiffness. On the other hand the elongation stiffness was large, resulting in negligible elongation of the ropes during the flume tank experiments.

To emulate potential influence of seine net dragging resistance on seine rope behaviour during haul back, two different situations were applied to both rope types during the flume tank experiment:

- High resistance case. At the connection point between the seine ropes two clumps each weighting 800 g was attached to a hinge.
- Low resistance case. Equipped with just the mounting hinge weighting 7 g at the connectiom point.

The experiments consisted of the three different initial layout patterns, two different seine rope types and two different winch speeds. This makes 24 different experimental haul back cases (Tab. 1).

TABLE 1: The 24 experimental cases conducted in the flume tank

Case no	Layout pattern	Rope type	Net Weight [g]	Winch Speed [m/s]
1	Square	Combination	7	0.157
2	Square	Combination	1607	0.157
3	Square	Combination	7	0.314
4	Square	Combination	1607	0.314
5	Square	Polyester	7	0.157
6	Square	Polyester	1607	0.157
7	Square	Polyester	7	0.314
8	Square	Polyester	1607	0.314
9	Diamond	Combination	7	0.157
10	Diamond	Combination	1607	0.157
11	Diamond	Combination	7	0.314
12	Diamond	Combination	1607	0.314
13	Diamond	Polyester	7	0.157
14	Diamond	Polyester	1607	0.157
15	Diamond	Polyester	7	0.314
16	Diamond	Polyester	1607	0.314
17	Triangle	Combination	7	0.157
18	Triangle	Combination	1607	0.157
19	Triangle	Combination	7	0.314
20	Triangle	Combination	1607	0.314
21	Triangle	Polyester	7	0.157
22	Triangle	Polyester	1607	0.157
23	Triangle	Polyester	7	0.314
24	Triangle	Polyester	1607	0.314

Motion tracking data for all these 24 cases were acquired during the flume tank experiments following the procedure described in the section above.

Simulation Model

The dynamics of the demersal seine gear is dominated by the behaviour of the seine ropes. Hence, the numeric simulation model was developed with two cables modelling the seine ropes, attached to a weight representing the seine net. There are several methods which can be used to represent cable mechanics in simulations such as presented in [9-15]. The demersal seine fishing is of dynamic nature and a time-domain formulation of the cable dynamics was required. The model implements the method found in [15], which contains a model where the cable dynamics are formulated as a collection of hinged rigid bodies.

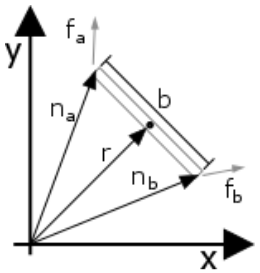

FIGURE 5: Constraint formulation of rigid body dynamics for a single element

A single rigid element can be defined by the vectors to the element end points, see Eqn. 1 and Fig. 5:

$$\boldsymbol{b} = \boldsymbol{n}_b - \boldsymbol{n}_a \tag{1}$$

And the translational dynamics of the element centre follows from Newton's 2nd law:

$$\ddot{\boldsymbol{r}} = \frac{1}{m}(\boldsymbol{f}_a + \boldsymbol{f}_b) \tag{2}$$

The rotational dynamics of the element can be expressed in terms of the rotational momentum:

$$\boldsymbol{h} = \int_V (\boldsymbol{r}_v \times \dot{\boldsymbol{r}}_v)\ \rho\ dV \tag{3}$$

$$\boldsymbol{h} = m\,\boldsymbol{b} \times \dot{\boldsymbol{b}} \int_{-\frac{1}{2}}^{\frac{1}{2}} \zeta^2 d\zeta \ \rightarrow \boldsymbol{h} = \frac{m}{12}\boldsymbol{b} \times \dot{\boldsymbol{b}} \tag{4}$$

$$\dot{\boldsymbol{h}} = \frac{m}{12}\left(\dot{\boldsymbol{b}} \times \dot{\boldsymbol{b}} + \boldsymbol{b}\ddot{\boldsymbol{b}}\right) = \frac{m}{6}\boldsymbol{b} \times \ddot{\boldsymbol{b}} = \boldsymbol{b} \times (\boldsymbol{f}_b - \boldsymbol{f}_a) \tag{5}$$

$\boldsymbol{b} \times \ddot{\boldsymbol{b}}$ is rank deficient and an additional equation is needed in order to fully specify the element dynamics. The additional equation takes the form of a constraint and the resulting set of equations is on the differential algebraic form. The equations can be formulated in the time-domain by double-differentiation, which in turn can be arranged as a set of coupled ordinary differential equations.

$$\boldsymbol{C}(\boldsymbol{q}) = 0 \tag{6}$$

$$\ddot{\boldsymbol{C}} = \boldsymbol{W}(\boldsymbol{q})\ddot{\boldsymbol{q}} + \dot{\boldsymbol{W}}(\boldsymbol{q})\dot{\boldsymbol{q}} = 0 \tag{7}$$

With the derivative of the constraint equation with respect to the degrees of freedom in the constraint defined as:

$$\boldsymbol{W}(\boldsymbol{q}) = \frac{\partial \boldsymbol{C}}{\partial \boldsymbol{q}} \tag{8}$$

The length of the element can be used as a constraint with $\boldsymbol{W}(\boldsymbol{q}) = \boldsymbol{b}^{\boldsymbol{T}}$.

$$\boldsymbol{C}_l = \boldsymbol{b}^T\boldsymbol{b} - L^2 = 0 \quad (9)$$
$$\dot{\boldsymbol{C}}_l = \boldsymbol{b}^T\dot{\boldsymbol{b}} - 2L\dot{L} = 0 \quad (10)$$
$$\ddot{\boldsymbol{C}}_l = \boldsymbol{b}^T\ddot{\boldsymbol{b}} + \dot{\boldsymbol{b}}^T\dot{\boldsymbol{b}} - 2L\ddot{L} - 2\dot{L}^2 = 0 \quad (11)$$

This gives the following for the rigid element dynamics:

$$\ddot{\boldsymbol{r}} = \frac{1}{m}(\boldsymbol{f}_a + \boldsymbol{f}_b) \quad (12)$$
$$\boldsymbol{b} \times \ddot{\boldsymbol{b}} = \frac{6}{m}\boldsymbol{b} \times (\boldsymbol{f}_b - \boldsymbol{f}_a) \quad (13)$$
$$\boldsymbol{b}^T\ddot{\boldsymbol{b}} = -\dot{\boldsymbol{b}}^T\dot{\boldsymbol{b}} + 2\left(L\ddot{L} + \dot{L}^2\right) \quad (14)$$

An advantage of the constraint formulation is that it may be used to formulate structural continuity between a set of rigid bodies. A discretized cable can be constructed by applying a constraint which imposes continuity between the endpoints as seen in Fig. 6 and Eqn. 15.

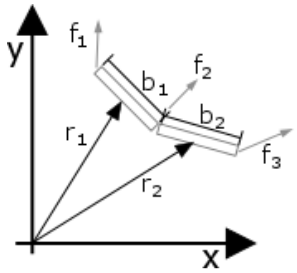

FIGURE 6: Constraint for continuity of a hinged structure

$$\boldsymbol{C}_c = \boldsymbol{r}_1 + \frac{1}{2}\boldsymbol{b}_1 + \frac{1}{2}\boldsymbol{b}_2 - \boldsymbol{r}_2 = 0 \quad (15)$$

The constraint equation will not be satisfied with two integration steps as time progresses. The error of the constraint equation can be eliminated by introduction of a control law which guarantees global asymptotic stability.

$$\ddot{\boldsymbol{C}}_l = \boldsymbol{u}_l \quad (16)$$
$$\boldsymbol{u}_l = -K_{dL}\dot{\boldsymbol{C}}_l - K_{pL}\boldsymbol{C}_l \quad (17)$$

The control law that ensures fulfilment of the constraint equation will introduce properties such as stiffness and damping to the composite structure. The control law is in the form of a linear system, or filter, and the constants can be chosen to represent any material and response dynamics. The frequency response of this system will also determine the response frequencies, or lack thereof, in the structure. A proper choice of parameters allows the formulation to admit low and medium frequency responses while attenuating high frequency oscillations. This is an important property when considering time domain integration schemes where numeric stability is closely related to the step size.

Model Implementation

The previously described model formulation was used to implement the simulation model for the seine ropes behaviour in the FhSim simulation framework [16]. Hence the seine ropes were modelled by cables consisting of a collection of six degree of freedom elements. The cables were connected to the weight at one end, representing the seine net, and to a winch at the other. The cables were initialized by a list of waypoints which specified the cable length between points in space. The rigid body elements were distributed along a catenary curve between these points. The simulation model as implemented in FhSim is seen in Fig. 7. The orientation of the catenary curve was smoothly rotated from vertical to horizontal near the bottom to avoid initializing cable segments beneath the bottom. The lump weight was modelled as a capsule geometry and initialized at the average end point of the cables.

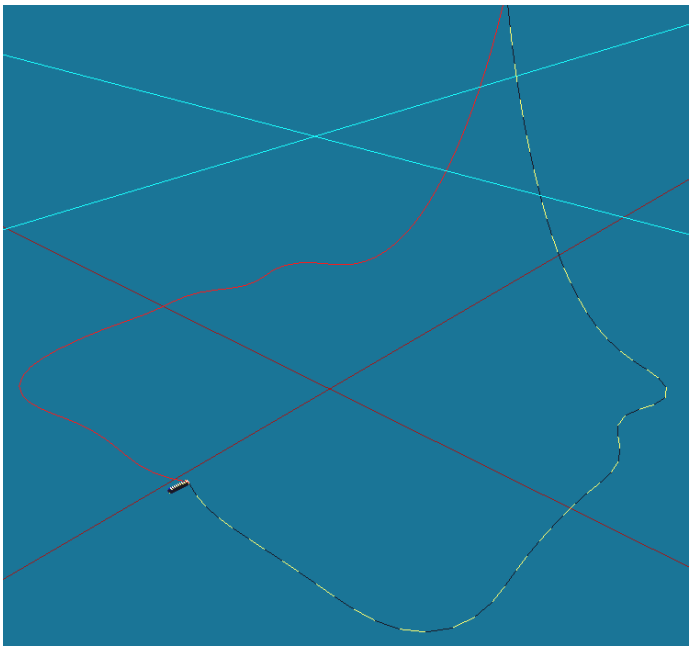

FIGURE 7: Numerical seine cable model shown in FhSim. The cables are retracted at the top of the image while the weight is seen in the lower left corner.

The simulation model used an existing bottom contact model from FhSim [16] which calculates a reaction force normal to the bottom from an overlap between element cylinder geometry and the flat bottom surface. The normal force results in a transversal friction force modelled by a friction coefficient with value in the range 0.0 to 1.0. Time integration was performed with a simple forward Euler scheme [17] and a time-step of 1e-3s.

The rigid body implementation of the cable assumes that each element consists of a homogenous and isotropic material. This assumption is violated by the weaved structure of seine ropes and the large difference between bending and axial stiffness observed was introduced in the model by a scaling of the material stiffness. The effective material stiffness in bending was scaled linearly from the axial stiffness.

Validation of the Simulation Model

Simulations of the flume tank experiments were conducted using the simulation model with cases defined by Tab. 1. The initial layout patterns for the simulation model were derived from node position data (positions of the reflective markers attached to the seine ropes) acquired at the start of the experiments. The ability of the simulation model to reproduce the kinematic behaviour seen in reality was assessed by comparison with experimental data from the flume tank. This was done by producing a sequence of 2D pictures which showed how the shape of the seine ropes and the encircled bottom area evolved during the haul back process in both experiments and simulations. This sequence of the kinematic behaviour was produced both from above and from the side, and the results from the experiments were overlaid on the simulation result plots. However the values for bottom friction and seine rope bending stiffness needed to be selected for the simulations as these properties were left unmeasured in the experiments. The bottom friction coefficient was selected by testing several different values and choosing a value which gave good agreement between simulations and the experimental results across the set of cases. The seine rope bending stiffness was fixed at a very small value since both types of ropes tested exhibited little resistance towards bending.

Predicting Seine Rope Behaviours

The validated simulation model was used to investigate both the effect of environmental properties and physical properties of the seine ropes on the gradual change in the encircled area. For each parameter a pair of values which were considerably different was selected. Then the haul back process was simulated starting from the same initial layout pattern. The sensitivity of the model to the parameters was assessed by subsequently overlaying corresponding plots from the two simulations. These were used to examine how, and to what extent, the kinematic behaviour of the seine rope and encircled area was affected by each parameter.

The effect of the bottom friction was investigated by means of the procedure described above. This parameter is of great importance since it can be used to model the effect of fishing on different seabed types and is one of the environmental parameters which to a large extent influence the real world performance of seine ropes. Seabed contact for seine ropes is important during demersal seining since it will affect the efficiency of herding the encircled fish into the seine net in the later stages of the fishing process. Therefore, the effect of the density of the seine rope was investigated since this might affect the extent of bottom contact during the haul back process. Finally, the effect of the seine rope bending stiffness was investigated as this property may affect the shapes the encircled area undertakes during the fishing process.

RESULTS

The results from the 24 experiments carried out in the flume tank are presented first. These results are used in order to compare the data collected from the experiments with data generated by simulations of the same experiments. This allows us to validate the seine rope model for the chosen parameters values for bottom friction and seine rope bending stiffness. Finally, we use comparisons of simulations versus simulations to show the predictive power of the simulation model.

Experimental Results

Fig. 8 shows results from the complete set of experiments performed (Tab. 1). Each of the 24 plots in Fig. 8 show the seine ropes as seen from above, it is the area encircled by the ropes. Each plot consists of 6 superimposed paths corresponding to the time development. The time between the pictures shown are 10 seconds for the first two columns, for the slow winch speeds. The last two columns are for the fast winch speed experiments. Here the time step between pictures is 5 seconds. Each picture corresponds to an area being 8 m wide and 9.5 m long. The odd rows are from combination rope experiments, the even rows from polyester rope. The odd columns show light net weight, even show heavy net weights. The layout patterns used in the experiment are shown with the top two rows as square, middle two rows as diamond and the bottom two rows as triangle.

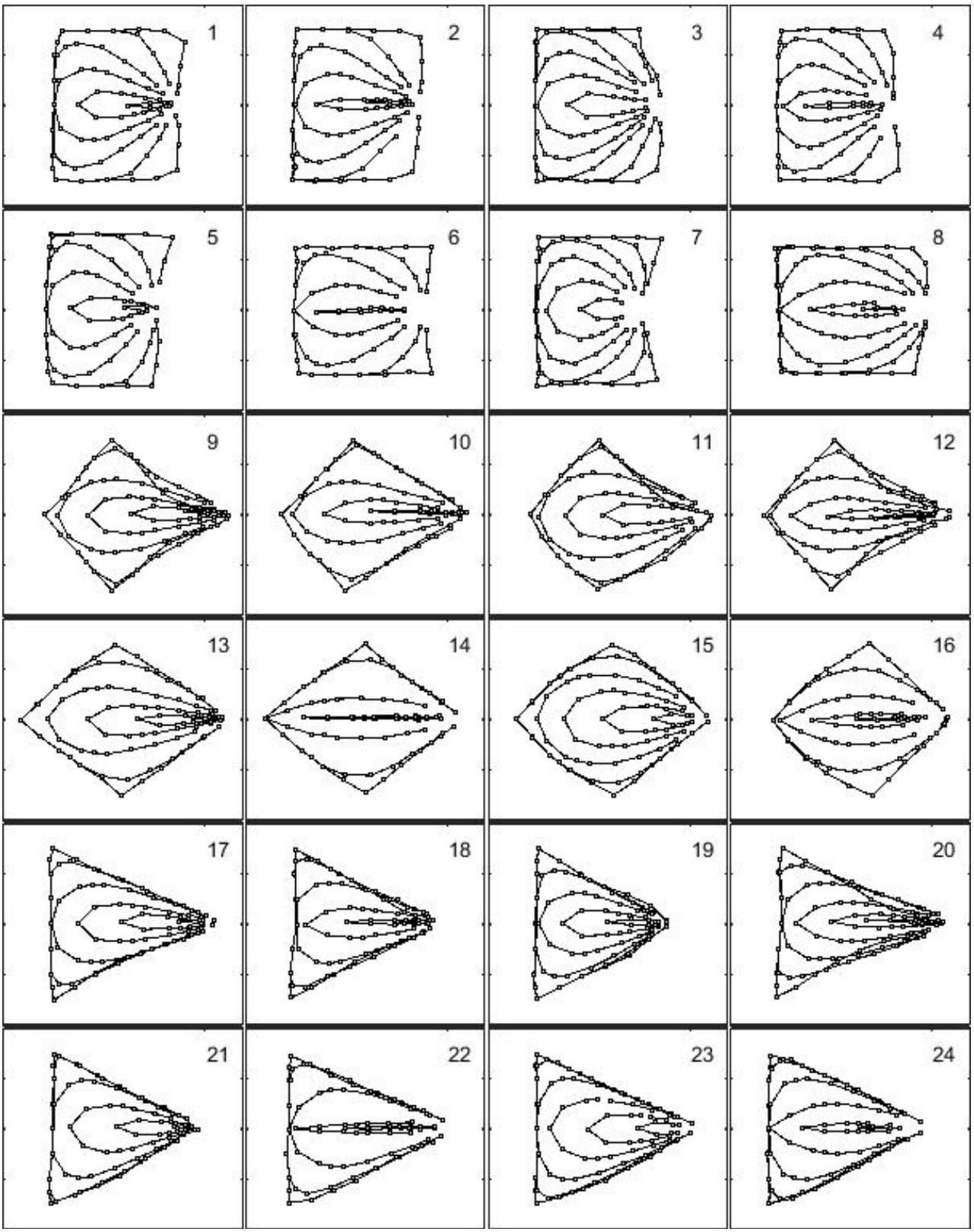

FIGURE 8: Odd rows: combination rope, even rows: polyester rope. Odd columns: light net weight, even columns: heavy net weight. The first two columns show slow winch speed, the last two columns fast winch speed. The dots show the positions of the reflective markers mounted on the seine ropes. The labels correspond to the experimental cases described in Tab. 1.

Flume Tank Experiments Compared to Simulation

The comparison of experiment against simulation was performed by extracting the initial position of all markers on the seine rope. This information was used as the initial condition in the simulation by initializing the cable with the positions as waypoints. The simulation was set up with a number of points of interests defined along the seine rope. These points of interest in the simulation were set up as to correspond to the reflective markers used in the flume tank. To validate the simulation model, we compare the position of the reflective markers to the points of interest. The haul back used in the experimental setup was not continuous at all times; there were some events where the seine rope slipped on the winch. This makes the comparison in the time domain difficult, but for the same amount of seine rope hauled in the comparison is possible. We present cases using different layout and differing seine rope properties.

Simulations were carried out for the three different layout patterns; square, diamond and triangle to be compared to the experiments with a combination rope, light weight and slow winch speed. This corresponds to the experimental cases: no 1, 9 and 17 in Tab. 1 and Fig. 8. In Fig. 9 we show the experimental results (circular markers) and the simulation (solid lines) seen from above and from the side. The plots are generated at eight seconds intervals for the square and triangle layout. The diamond layout is shown with a plot interval of six seconds.

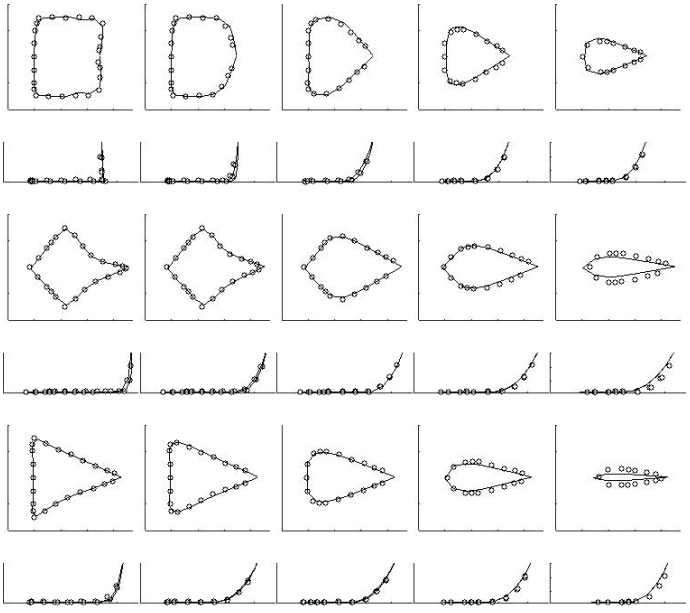

FIGURE 9: Simulations (solid lines) compared to flume tank experiments (circular markers) for the three different initial layout patterns: square (top), diamond (centre), triangle (bottom). The time steps in the "movie clips" are 6 seconds for the diamond pattern while it is 8 seconds for the two other. Experimental case 1, 9 and 17 (Tab. 1 and Fig. 8).

The comparison shows a large degree of correspondence for the initial four frames. The last frame shows some disagreement between simulations and measurements for the diamond and triangle layout patterns. This could be due to problems with uneven hauling speed accumulating errors evident at the end of the experiments.

Simulations were also carried out for a combination rope and a polyester rope. A heavy weight, a slow speed and the square layout was chosen for this comparison. This corresponds to the experimental cases: no 2 and 6 in Tab. 1 and Fig. 8. In Fig. 10 we show the result of the comparison with 10 seconds intervals. It is seen from the figure that the simulation is a better match in the case of the combination rope.

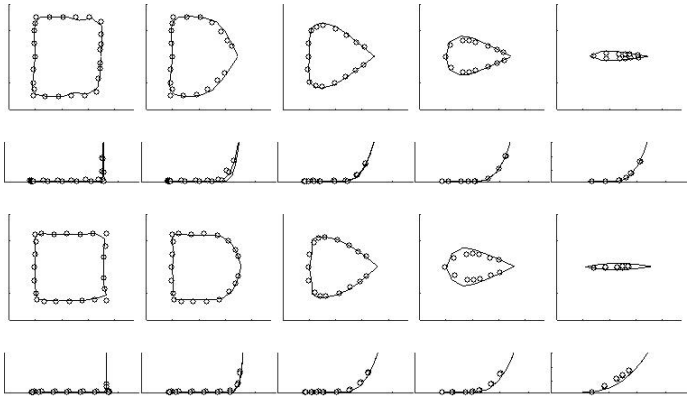

FIGURE 10: The top rows show the combination rope with interval of 10 seconds. The bottom rows the polyester rope, also with 10 seconds intervals. The lines represent simulations while the dots represent the flume tank results. Experimental case 2 and 6 (Tab. 1 and Fig. 8).

The simulated results shown in Fig. 9 and 10 are all based on scaling the bending stiffness by a factor 2.0e-3 compared to what would be expected based on the Timoshenko beam theory [18]. Using such a low value for the bending stiffness makes perfectly sense based on the observations made during the flume tank experiments that ropes applied was very flexible regarding bending stiffness. For the friction between the ropes and flume tank floor we found that a value at 0.5 provided the best overall agreement between simulated and experimental results. Therefore this value is applied for the simulated results shown in Fig. 9 and 10. Since both seine rope types tested in the flume tank had an outer layer of polyester and the flume tank floor is covered by a nylon carpet we would expect a friction coefficient in the range 0.3-0.5 [19]. The value we found to give the best correspondence between simulated and experimental results is therefore within the expected range.

Predictions Based on Simulation

Simulation results in this section show the result of systematic variation of the friction coefficient and bending stiffness parameters of the seine ropes.

Variation in rope and lumped mass weight. The difference between combination rope and a polyester rope was investigated with the slow winch speed (0.157 m/s) for a diamond layout pattern. The result for a 161g weight is shown in Fig. 11 with circular markers for the combination rope and a solid line for the polyester rope. Fig. 11 shows little difference in the kinematic behaviour between the two rope materials.

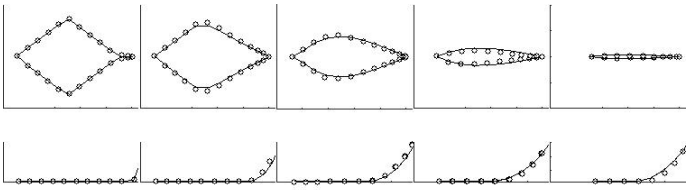

FIGURE 11: Simulated seine rope behaviour for combination rope (circles) vs. polyester (lines). The net weight was fixed at 161g**.**

A tenfold increase in lumped mass weight to 1.6 Kg produced the simulation results shown in Fig. 12. Here the difference is pronounced where the seine ropes lift off the bottom as they are hauled in for the lighter polyester rope, whereas the heavier combination rope maintains bottom contact for a larger proportion of the process.

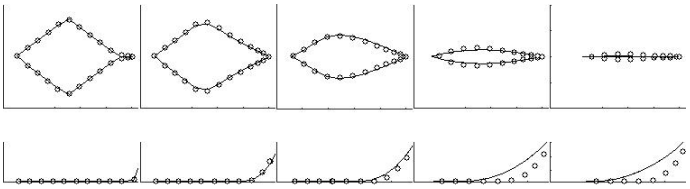

FIGURE 12: Simulated seine rope behaviour for combination rope (circles) vs. polyester rope (line). The net weight was fixed at 1.6 kg.

Variation of the friction coefficient against the bottom. The friction coefficient experienced by demersal seine ropes will depend on the conditions of the seabed. Hence it is relevant to investigate the effect of bottom friction on the behaviour of the seine ropes. The influence of the friction coefficient was investigated by simulation of the combination rope since it experienced more bottom contact than the lighter polyester rope. The weight for the net was set to 161g. The haul back speed of the winch was set to 0.157 m/s and the friction coefficient was varied between 0.25 and 1 in steps of 0.25 (Fig. 13).

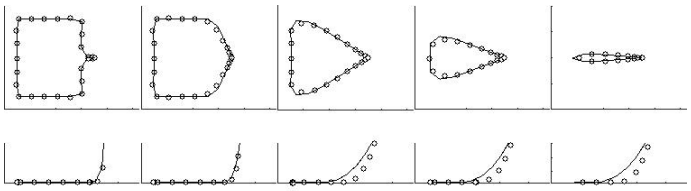

FIGURE 13: Simulation with friction coefficient set at 0.25 (dots) versus set at 1.0 (lines) for the combination rope. Net weight was fixed at 161g.

Variation of the bending stiffness scale. We simulated a combination rope with a 1.6 Kg weight attached and a winch speed of 0.157 m/s. The bending stiffness scale used to mimic the non-isotropic material was varied from 2e-3 to 1e-1. A special round-shaped initial layout pattern was applied for investigating the effect of seine rope bending stiffness to avoid a non-physical start shape for the simulation with a large bending stiffness (1e-1). Fig. 14 shows the simulated seine rope behaviour with 10 seconds interval between pictures. The stiffer rope forces the net backwards as the ropes is hauled in. The rope with the small bending stiffness maintains a larger encircled area during the haul back, as is evident from the 5th plot in Fig. 14. Seen from the side we see a small tendency for the rope to lift off the seabed earlier for the stiffer rope.

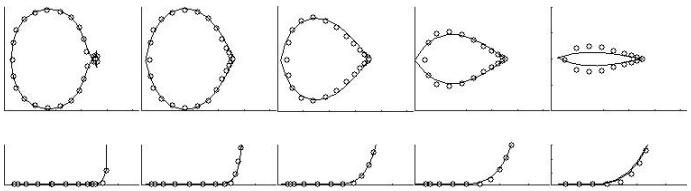

FIGURE 14: Simulated seine rope behaviour for a combination rope assuming bending stiffness scale at 2e-3 (dots) versus 1e-1 (lines). The net weight was fixed at 1.6 kg.

The three predictive cases show that the simulation model is sensitive to variations in the input parameters.

DISCUSSION

This paper has presented flume tank experiments for the kinematic behaviour of seine ropes laid out in different initial patterns. Ropes with considerable different densities were tested and the seine net resistance was modelled by attaching a weight to the connection point between the two seine ropes. The results obtained from the different cases tested in the flume tank were then applied to validate a physical model for simulation of seine ropes behaviour when deployed for demersal seining. The comparison between the flume tank experiments and the similar simulation cases showed that the simulation model was able to reproduce the kinematic behaviour of the different seine ropes configurations tested with high accuracy for the three initial layout patterns. Based on these results and given that the simulation model is created

from a first principles approach for structural dynamics, fluid dynamics and bottom contact (flume tank floor), we are confident to apply this model for predictions outside the range of the presented validation cases. In particular this means that we should be able to apply our dynamic seine rope simulation model to investigate the behaviour of real seine ropes which compared to in configurations tested in the flume tank easily can be more than a factor 100 longer [3, 4]. The dimensions of real seine ropes applied in demersal seining makes simulations the only realistic option for investigating extensively the kinematic and dynamic behaviour of the fishing gear during operations. In this respect the validated simulation model provide new options for studying the demersal seine fishing process by means of simulation. Studying the physical behaviour of active fishing gears by means of numerical modelling and simulation is well-known in literature especially for trawl fishing [11] and [13]. However these studies on trawls have applied a steady state modelling approach since the geometry of trawls tend to have a static shape during most of the fishing process. This makes the steady state a realistic simplification for use in trawl fisheries but the dynamic nature of demersal seining excludes steady state as a useful description of fishing operations. This is a particular issue for the seine ropes due to changing shape of the encircled area and the fishing methods integral use of the herding effect of the ropes. The simulation model validated in this article is therefore dynamic in its formulation and to our knowledge this work is the first time a simulation model for seine rope behaviour has been validated through flume tank experiments.

ACKNOWLEDGMENTS

The investigations included in this study were funded by the Research Council of Norway (project no. 225193 (MAROFF-2)) and the Norwegian Seafood Research Fund (project no. 900861 (FHF)). We are grateful for their financial support.

REFERENCES

[1] Norges Råfisklag. http://www.råfisklaget.no.

[2] J.C. Sainsbury. *Commercial fishing methods. An Introduction to vessels and gears.* Fishing News Books. Wiley, August 1996.

[3] Fisheries Research and Development Corporation http://fish.gov.au/ fishing_methods/Pages/nets.aspx

[4] Bent Herrmann, Roger B. Larsen, Manu Sistiaga, Nina A.H. Madsen, Karl G. Aarsæther, Eduardo Grimaldo, Olafur A. Ingolfsson, 2014. *Quantifying Size Selection of Cod (Gadus morhua) in Square Mesh Codends for Demersal Seining: a Simulation-based Approach.* Sintef report A26515 (ISBN 978-82-14-05774-4).

[5] SINTEF Fisheries and Aquaculture. http://www.sintef.dk.

[6] SINTEF Fisheries and Aquaculture. *Fact Sheet: The North Sea Centre Flume Tank.* http://www.sintef.no/globalassets/upload/fiskeri_og_havbruk/faktaark/Flumetank_eng.pdf.

[7] Qualisys Track Manager http://www.qualisys.com/products/software/qtm

[8] Gonzales, R.C., Wintz, P., 1987. *Digital Image Processing.* Addison-Wesley Publishing Company. ISBN 0-201-11026-1

[9] Desai, Chandrakant S., and John F. Abel. *Introduction to the finite element method: a numerical method for engineering analysis*. Van Nostrand Reinhold, 1972.

[10] Zienkiewicz, Olek C., and Robert L. Taylor. *The finite element method for solid and structural mechanics.* Butterworth-heinemann, 2005.

[11] Priour, D. *"FEM modeling of flexible structures made of cables, bars and nets."*Maritime Transportation and Exploitation of Ocean and Coastal Resources Guedes Soares, Garbatov and Fonseca (eds) Taylor and Francis Group, London, ISBN 0 415.39036 (2005): 2.

[12] Driscoll, F R and Lueck, R G and Nahon, M, *Development and validation of a lumped-mass dynamics model of a deep-sea ROV system,* Applied Ocean Research, 2000.

[13] Khaled, Ramez, Daniel Priour, and Jean-Yves Billard. *"Cable length optimization for trawl fuel consumption reduction."* Ocean Engineering 58 (2013): 167-179.

[14] Reite, Karl Johan. *"Modeling and control of trawl systems."* PhD thesis, ISBN 82-471-8023-5, NTNU, 2006.

[15] Vegar Johansen. *Modelling of Flexible Slender Systems for Real-Time Simulation and Control Application.* PhD thesis, ISBN 978-82-471-4915-7, NTNU, December 2007.

[16] Karl-Johan Reite, Martin Føre, Karl Gunnar Aarsæther, Jørgen Jensen, Per Rundtop, Lars T. Kyllingstad, Per Christian Endresen, David Kristiansen, Vegar Johansen and Arne Fredheim. *Fhsim - Time Domain Simulation of Marine Systems.* In ASME 2014 33rd International Conference on Ocean, Offshore and Arctic Engineering, volume 8A: Ocean Engineering. Ocean, Offshore and Arctic Engineering Division, 2014.

[17] Egeland, O., & Gravdahl, J. T. (2002). *Modeling and simulation for automatic control*. Marine Cybernetics, Trondheim, Norway, ISBN 82-92356-00-2.

[18] Timoshenko, S.P., Goodier, J.N., 1982. Theory of Elasticity. McGraw-Hill, ISBN: 07-085805-5.

[19] http://www.heimbach.com.

